

# Normalization of quasinormal modes in leaky optical cavities and plasmonic resonators

Philip Trøst Kristensen

*Institut für Physik, Humboldt Universität zu Berlin, 12489 Berlin, Germany*

Rong-Chun Ge and Stephen Hughes

*Department of Physics, Queen's University, Kingston, Ontario K7L 3N6, Canada*

(Dated: December 7, 2024)

We discuss three formally different formulas for normalization of quasinormal modes currently in use for modeling optical cavities and plasmonic resonators and show that they are complementary and provide the same result. Regardless of the formula used for normalization, one can use the norm to define an effective mode volume for use in Purcell factor calculations.

## I. INTRODUCTION

Optical cavities and plasmonic resonators enable tight localization of optical fields to length scales on the order of the wavelength or shorter. In addition, the resonant nature of these material systems suggest that the possible electromagnetic waves should be discrete, similar to the bound states of the hydrogen atom. The analogy is somewhat deceptive because electromagnetic resonators are inherently leaky, resulting in a continuous dissipation of energy via radiation or absorption in the material. Nevertheless, distinct resonances show up as peaks in spectra from scattering calculations or measurements, for example, in which the width of the peak is related to a finite lifetime due to the dissipation of energy; the associated scattered fields often show signatures of an underlying modal structure.

In computational nanophotonics, the optical or plasmonic response of resonant systems are often modeled by use of time-domain calculations with Perfectly Matched Layers (PMLs) and a run-time Fourier transform to extract the modal field distribution. This technique has

been very successful for modeling high quality optical cavities for which the spectral resonances are well separated. In particular, the modes so calculated have been used for estimates of the spontaneous emission rate enhancement via the Purcell formula<sup>1</sup>, from which the spontaneous emission rate is expected to scale with the ratio of the cavity quality factor  $Q$  to the effective mode volume  $V_{\text{eff}}$ . The effective mode volume describes the degree of light localization in the cavity and has a clear definition for closed resonators in terms of the integrated energy density of light in the mode. The definition, however, cannot be directly extended to dissipative systems for which the mode extends over all space, and this has conceptual consequences for the application of the Purcell formula which manifestly pertains to dissipative systems with a finite  $Q$  value. Theoretically, the response of dissipative resonant structures can be understood in terms of so-called quasinormal modes<sup>2–4</sup> (QNMs), which appear as discrete solutions to the wave equation that satisfy a radiation condition compatible with the propagation of light away from the resonator. Figure 1 shows an example of a plasmonic resonator, in the form of a nanorod dimer, and the field profile of the fundamental QNM in the dimer. The use of PMLs is one possible realization of a radiation condition for resonators in homogeneous media, wherefore it was pointed out in Ref. 5 that the optical cavity modes commonly calculated by time-domain techniques are exactly the QNMs, and that the Purcell formula can be derived within a QNM framework such as developed in Refs. 6–10, for example; this leads naturally to a definition of the effective mode volume which is compatible with the leaky nature of the modes. The effective mode volume is intimately connected with the normalization of the QNMs, and two alternative formulations of the effective mode volume were derived in Refs. 11 and 12 based on different formulations of the norm. In this article we show how the three different normalization integrals are closely related and provide the same result. In essence, we show that the differences in the formulas can be understood as alternative regularization procedures for an inherently ill-behaved integral. Although we illustrate the formal connection between the three formulations, it is worth

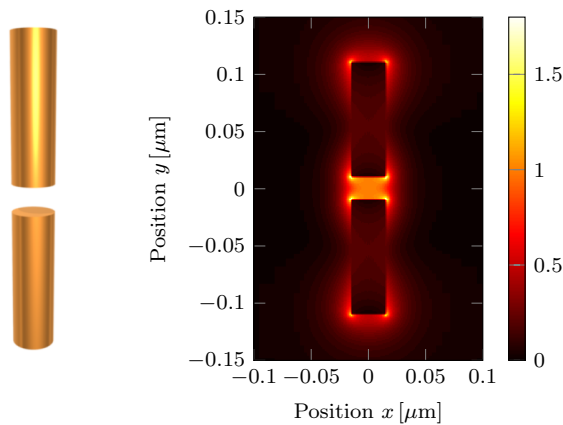


FIG. 1: Left: Illustration of a gold nanorod dimer. Right: Absolute value of the fundamental QNM  $\tilde{\mathbf{f}}_c(\mathbf{r})$  in the plane  $z = 0$ . The QNM is scaled to unity at the position  $\mathbf{r}_c = (0, 0, 0)$  in the center between the two rods.

emphasizing that they were derived by use of very different approaches in Refs. 6,11 and 13. The equivalence of the formulas, therefore, should be regarded as a profound strength of the entire modeling framework for localized electromagnetic resonators based on QNMs.

The article is organized as follows: In section II we introduce the three formulations of the QNM norm and discuss how they relate to each other. Section III provides explicit example calculations to illustrate the practical evaluation as well as the equivalence of the norms. Section IV summarizes and concludes the article.

## II. NORMALIZATION INTEGRALS

We consider electric field QNMs  $\tilde{\mathbf{f}}_\mu(\mathbf{r})$  of resonators embedded in a homogeneous background defined as the eigenmodes of Maxwell's wave equation

$$\nabla \times \nabla \times \tilde{\mathbf{f}}_\mu(\mathbf{r}) - \tilde{k}_\mu^2 \epsilon_r(\mathbf{r}) \tilde{\mathbf{f}}_\mu(\mathbf{r}) = 0, \quad (1)$$

in which  $\tilde{k}_\mu = \tilde{\omega}_\mu/c$  is the ratio of the angular resonance frequency to the speed of light and  $\epsilon_r(\mathbf{r})$  is the relative permittivity. Because of the leaky nature of the resonators, the differential equation should be augmented by a radiation condition to only allow outgoing wave solutions at large distances. For the case of a homogeneous environment, we argue that this radiation condition is formally the Silver-Müller radiation condition<sup>14</sup> in the form

$$\frac{\mathbf{r}}{r} \times \nabla \times \tilde{\mathbf{f}}_\mu \rightarrow -in_B \tilde{k}_\mu \tilde{\mathbf{f}}_\mu \quad \text{as } r \rightarrow \infty, \quad (2)$$

where  $n_B$  is the refractive index of the homogeneous background material. The Silver-Müller radiation condition is commonly imposed to correctly model scattered fields. Therefore, we argue that this is also the radiation condition for the QNMs, which can be considered solutions to the scattering problem with no source. Because it is defined only in the limit of infinite distances, Eq. (2) is rarely useful in numerical calculations of QNMs. Instead, one can use PMLs to mimic the radiation condition by removing reflections from the calculation domain boundary, or one can use calculation methods based on the Green tensor which expressly respects the radiation condition. As a result of the radiation condition the differential equation problem becomes non-Hermitian, wherefore a number of well-known text book results for Hermitian eigenvalue problems do not apply. In particular, the resonance frequencies  $\tilde{\omega}_\mu = \omega_\mu - i\gamma_\mu$  are complex with a negative imaginary part, from which the  $Q$  value can be calculated as  $Q_\mu = \omega_\mu/2\gamma_\mu$ .

The complex resonance frequencies in combination with the radiation condition leads to a divergent behavior of the QNMs as a function of distance from the resonator and makes the normalization non-trivial. As discussed in the introduction, the problem of normalization for QNMs has been addressed by at least three different methods leading to three different formulas that we discuss in de-

tail below. Before moving on, however, it is worth elaborating a bit on the connection between the mathematical concept of the norm, and the more physical concept of mode volume. Regardless of the formula used for normalization, one can use the norm to define a generalized effective mode volume for the QNM of interest (denoted by  $\mu = c$ ) as<sup>5</sup>

$$v_c = \frac{\langle \tilde{\mathbf{f}}_c | \tilde{\mathbf{f}}_c \rangle}{\epsilon_r(\mathbf{r}_c) \tilde{\mathbf{f}}_c^2(\mathbf{r}_c)}, \quad (3)$$

where  $\langle \tilde{\mathbf{f}}_c | \tilde{\mathbf{f}}_c \rangle$  denotes the QNM norm (in any formulation compatible with the properties of the QNMs),  $\mathbf{r}_c$  denotes the center of the cavity, and  $\tilde{\mathbf{f}}_c^2(\mathbf{r}_c) = \tilde{\mathbf{f}}_c(\mathbf{r}_c) \cdot \tilde{\mathbf{f}}_c(\mathbf{r}_c)$ . The position  $\mathbf{r}_c$  denotes a point of special interest to the given resonator. For optical cavities, this will often be the center of the cavity in which the field is largest, and the generalized effective mode volume then gives a measure for the maximum light-matter interaction that one can obtain in the cavity. For general resonators there may be no unique way of defining the center, or it may be that the mode vanishes at this point. For plasmonic resonators, in particular, the field may be several orders of magnitude larger at the edges than within the material. Despite the large field values, however, the edges are often uninteresting for light-matter interaction because of enormous non-radiative decay and quenching. In general, therefore, we specify  $\mathbf{r}_c$  explicitly for each resonator.

The generalized effective mode volume is complex in general, and is related to the effective mode volume  $V_{\text{eff}}$  of the Purcell formula as

$$\frac{1}{V_{\text{eff}}} = \text{Re} \left\{ \frac{1}{v_c} \right\}. \quad (4)$$

This definition follows directly and quite naturally from a derivation of the original Purcell formula in the framework of QNMs, either using a Green tensor approach<sup>4,12</sup> or a mode expansion formulation<sup>11</sup>. It follows from these derivations, that the usefulness of the effective mode volume for Purcell factor calculations is restricted to material systems or frequency ranges for which a single mode dominates the response. Moreover, the use of Eq. (4) in Purcell factor calculations is valid in the limit  $\tilde{\omega}_c/\omega_c \approx 1$  which may not hold for very low- $Q$  optical cavities or plasmonic resonators. In cases where it does not hold, one can still recover the Purcell formula by redefining either Eq. (3) or (4), but it may be easier to calculate the spontaneous emission enhancement directly from a QNM expansion of the Green tensor. For plasmonic structures, the usefulness of the original Purcell formula is further limited by non-radiative decay channels at positions very close to the material<sup>15,16</sup>.

### A. Normalization by Lai *et al.*

For spherically symmetric resonators and non-dispersive materials, Lai *et al.*<sup>6</sup> introduced the normal-

ization

$$\langle\langle\tilde{\mathbf{f}}_\mu|\tilde{\mathbf{f}}_\mu\rangle\rangle_{\text{Lai}} = \lim_{V\rightarrow\infty} \left\{ \int_V \epsilon_r(\mathbf{r}) \tilde{\mathbf{f}}_\mu(\mathbf{r}) \cdot \tilde{\mathbf{f}}_\mu(\mathbf{r}) dV + i \frac{n_B}{2\tilde{k}_\mu} \int_{\partial V} \tilde{\mathbf{f}}_\mu(\mathbf{r}) \cdot \tilde{\mathbf{f}}_\mu(\mathbf{r}) dA \right\}, \quad (5)$$

where  $V$  is a spherical volume with boundary  $\partial V$  and  $dV$  and  $dA$  are differential volume and area elements, respectively. The normalization in Eq. (5) appears to date back to early work by Zel'dovich on the theory of unstable states<sup>17</sup>. This normalization was later adopted for general, leaky optical cavities in Ref. 5. The formula can be extended to dispersive resonators in homogeneous non-dispersive surroundings by the substitution<sup>7</sup>  $\epsilon_r(\mathbf{r}) \rightarrow \sigma(\mathbf{r}, \tilde{\omega}_\mu)$ , where

$$\sigma(\mathbf{r}, \omega) = \frac{1}{2\omega} \frac{\partial}{\partial \omega} (\omega^2 \epsilon_r(\mathbf{r}, \omega)). \quad (6)$$

For any resonator, we can evaluate the norm in Eq. (5) by first integrating over a spherical domain  $V_0$  of radius  $R_0$  completely enclosing the resonator; clearly, this integral can be easily evaluated. For the region  $r > R_0$ , we can write the QNMs in terms of spherical Hankel functions  $h_l(n_B \tilde{k}_\mu r)$  and vector spherical harmonics<sup>18</sup>. The vector spherical harmonics are orthogonal with respect to integration over all angles<sup>18</sup>, wherefore the norm may be rewritten in the form

$$\langle\langle\tilde{\mathbf{f}}_\mu|\tilde{\mathbf{f}}_\mu\rangle\rangle_{\text{Lai}} = \int_{V_0} \epsilon_r(\mathbf{r}) \tilde{\mathbf{f}}_\mu(\mathbf{r}) \cdot \tilde{\mathbf{f}}_\mu(\mathbf{r}) dV + \sum_{lm} I_l^r I_{lm}^\Omega, \quad (7)$$

in which

$$I_l^r = \lim_{R\rightarrow\infty} \left\{ \int_{R_0}^R n_B^2 h_l^2(n_B \tilde{k}_\mu r) r^2 dr + i \frac{n_B}{2\tilde{k}_\mu} h_l^2(n_B \tilde{k}_\mu R) R^2 \right\}, \quad (8)$$

and  $I_{lm}^\Omega$  includes the angular integration of the vector spherical harmonics, which is independent of  $R$  (and finite). The argument (originally by Lai *et al.*<sup>6</sup>) is now, that because of the outgoing wave nature of the Hankel functions at large distances, the increase in the volume integral is exactly balanced by the additional surface integral. For large arguments, the spherical Hankel functions tend to the limiting form

$$h_l(z) \rightarrow e^{-i\pi(l+1)/2} \frac{1}{z} e^{iz}, \quad z \rightarrow \infty, \quad (9)$$

so that inserting in Eq. (8) and differentiating with respect to  $R$  we find

$$\begin{aligned} \frac{d}{dR} I_l^r &= (-1)^{(l+1)} \frac{1}{\tilde{k}_\mu^2} \left\{ e^{2in_B \tilde{k}_\mu R} + \frac{i}{2n_B \tilde{k}_\mu} \frac{d}{dR} \left( e^{2in_B \tilde{k}_\mu R} \right) \right\} \\ &= 0, \end{aligned} \quad (10)$$

suggesting that one can assign a well-defined value to the norm as  $R \rightarrow \infty$ .

In practice, direct application of Eq. (5) leads to an

integral that seems to quickly converge towards a finite value, but in fact oscillates about this value with an amplitude that eventually starts to grow (exponentially) with the distance, albeit slowly compared to the length scales in typical calculations. This was noted in Ref. 5, where the oscillations were observed only for the cavity with the lowest quality factor ( $Q \approx 16$ ). The source of the oscillating integral can be traced back to the complex resonance frequency, which means that the wavenumber  $\tilde{k}_\mu$  is complex as well. Evaluation of Eq. (8) then leads to residual radius dependent terms of the form

$$f_{\text{Lai}}^{\text{res}}(R) = \sum_n \frac{1}{P_n(R)} e^{2in_B \tilde{k}_\mu R}, \quad (11)$$

where  $P_n(R)$  denotes general polynomials in  $R$  of order  $n > 0$ ; the surface term in Eq. (8) cancels the zero'th order term. Thus, while Eqs. (9) and (10) appear to be formally correct also for complex arguments, the limit  $R \rightarrow \infty$  in practice leads to a position dependent phase difference between the Hankel function and its limiting form, which makes the limit non-trivial to perform along the real axis. In principle, however, one can regularize the integral using coordinate transforms; a technique that has been used also for normalization of leaky modes in waveguides<sup>19</sup>. Formally, we can rewrite the integral as

$$\begin{aligned} I_l^r &= \lim_{R\rightarrow\infty} \left\{ \int_{R_0}^R n_B^2 h_l^2(n_B \tilde{k}_\mu r) r^2 dr + i \frac{n_B}{2\tilde{k}_\mu} h_l^2(n_B \tilde{k}_\mu R) R^2 \right. \\ &\quad \left. - \int_{R_0}^R \partial_r f_{\text{Lai}}^{\text{res}}(r) dr + \int_{R_0}^R \partial_r f_{\text{Lai}}^{\text{res}}(r) dr \right\} \\ &= F_l(R_0) + f_{\text{Lai}}^{\text{res}}(R_0) + \lim_{R\rightarrow\infty} \int_{R_0}^R \partial_r f_{\text{Lai}}^{\text{res}}(r) dr, \end{aligned} \quad (12)$$

where

$$F_l(r) = -\frac{r^3 n_B^2}{2} \left( h_l^2(n_B \tilde{k}_\mu r) - h_{l-1}(n_B \tilde{k}_\mu r) h_{l+1}(n_B \tilde{k}_\mu r) \right) \quad (13)$$

is the antiderivative of  $f_l(r) = n_B^2 h_l^2(n_B \tilde{k}_\mu r) r^2$ . In the last integral, we can now change the integration contour by writing  $r = R_0 + iz$  to find  $I_l^r = F_l(R_0)$ . For the case of a spherical resonator, we provide an example of this approach in section III A. Obviously, this regularization approach is rather cumbersome unless the expansion in spherical wave functions is explicitly known; also, it is rarely necessary in practice. Although the integral oscillates as a function of calculation domain size, the associated uncertainty in the calculated norm is much lower than the general numerical uncertainty for most QNM calculations. We elaborate on this issue in sections III B and III C.

## B. Normalization by Sauvan *et al.*

Sauvan *et al.*<sup>11</sup> used a different approach based on the Lorentz reciprocity theorem to introduce a normalization

for QNMs in general dispersive and possibly magnetic materials. For isotropic and non-magnetic materials, we may write the norm in terms of the electric field QNMs only as

$$\langle \tilde{\mathbf{f}}_\mu | \tilde{\mathbf{f}}_\mu \rangle_{\text{Sauvan}} = \frac{1}{2} \int_V \eta(\mathbf{r}, \tilde{\omega}_\mu) \tilde{\mathbf{f}}_\mu(\mathbf{r}) \cdot \tilde{\mathbf{f}}_\mu(\mathbf{r}) + \frac{1}{\tilde{k}_\mu^2} (\nabla \times \tilde{\mathbf{f}}_\mu(\mathbf{r})) \cdot (\nabla \times \tilde{\mathbf{f}}_\mu(\mathbf{r})) dV, \quad (14)$$

where  $\eta(\mathbf{r}, \omega) = \partial_\omega(\omega \epsilon_r(\omega, \mathbf{r}))$ ; for dispersionless materials this factor reduces to  $\eta(\omega, \mathbf{r}) = \epsilon_r(\mathbf{r})$ . This normalization seems to originate from the theory of leaky modes in waveguides<sup>20</sup>. In the original formulation and implementation in Ref. 11, there is no explicit requirement of the volume to tend to infinity. Instead, the integral is performed over both the usual calculation domain and the surrounding PMLs in which the real space coordinates are rotated into the complex plane, causing the propagating waves to decrease exponentially.

The correspondence with the normalization of Lai *et al.* was shown in Ref. 16, and is repeated here for the sake of completeness. First, we use the vector generalization of Green's identity of the first kind<sup>21</sup>,

$$\int_V (\nabla \times \mathbf{P}) \cdot (\nabla \times \mathbf{Q}) - \mathbf{P} \cdot \nabla \times \nabla \times \mathbf{Q} dV = \int_{\partial V} \mathbf{n} \cdot (\mathbf{P} \times \nabla \times \mathbf{Q}) dA, \quad (15)$$

to rewrite the integral as

$$\langle \tilde{\mathbf{f}}_\mu | \tilde{\mathbf{f}}_\mu \rangle_{\text{Sauvan}} = \frac{1}{2} \int_V \eta(\mathbf{r}, \tilde{\omega}_\mu) \tilde{\mathbf{f}}_\mu(\mathbf{r}) \cdot \tilde{\mathbf{f}}_\mu(\mathbf{r}) + \frac{1}{\tilde{k}_\mu^2} \tilde{\mathbf{f}}_\mu(\mathbf{r}) \cdot \nabla \times \nabla \times \tilde{\mathbf{f}}_\mu(\mathbf{r}) dV + \frac{1}{2\tilde{k}_\mu^2} \int_{\partial V} \mathbf{n} \cdot (\tilde{\mathbf{f}}_\mu(\mathbf{r}) \times \nabla \times \tilde{\mathbf{f}}_\mu(\mathbf{r})) dA. \quad (16)$$

Then, using the wave equation and Eq. (2) in the limit  $V \rightarrow \infty$ , we recover Eq. (5) with the substitution  $\epsilon_r(\mathbf{r}) \rightarrow \sigma(\mathbf{r}, \tilde{\omega}_\mu)$ . Importantly, the integrand in Eq. (14) is invariant under the coordinate transformations of the PMLs<sup>11</sup>. Therefore, the integral must have a well-defined value also under the trivial transformation where no coordinate rotation is performed<sup>16</sup>. In view of Eq. (16), this argument is a complement to Eq. (10) in suggesting that the norm has a well-defined value as  $R \rightarrow \infty$ .

### C. Normalization by Muljarov *et al.*

Muljarov *et al.*<sup>12,13</sup> derived a normalization which is similar in structure to Eq. (5), but with a different surface

term,

$$\langle \tilde{\mathbf{f}}_\mu | \tilde{\mathbf{f}}_\mu \rangle_{\text{Muljarov}} = \int_V \sigma(\mathbf{r}, \tilde{\omega}_\mu) \tilde{\mathbf{f}}_\mu(\mathbf{r}) \cdot \tilde{\mathbf{f}}_\mu(\mathbf{r}) d\mathbf{r} + \frac{1}{2\tilde{k}_\mu^2} \int_{\partial V} \tilde{\mathbf{f}}_\mu(\mathbf{r}) \cdot \partial_s (r \partial_r \tilde{\mathbf{f}}_\mu(\mathbf{r})) - r (\partial_r \tilde{\mathbf{f}}_\mu(\mathbf{r})) \cdot (\partial_s \tilde{\mathbf{f}}_\mu(\mathbf{r})) dA, \quad (17)$$

where  $\sigma(\mathbf{r}, \omega)$  is defined in Eq. (6), and  $\partial_s$  denotes the gradient in the direction normal to the surface of the volume  $V$ , which needs not be spherical and needs not extend to infinity. Comparing to the two other formulas, Eq. (17) makes explicit reference to a spherical coordinate system, the center of which one is left free to choose.

For the case of a spherical domain of radius  $R_0$ , we can show the correspondence with the normalization of Lai *et al.* by first evaluating the integrals  $I_l^r$  in Eq. (12) using the recurrence relations

$$h_{l-1}(kr) = \frac{l+1}{kr} h_l(kr) + \frac{1}{k} \partial_r h_l(kr) \quad (18)$$

$$h_{l+1}(kr) = \frac{l}{kr} h_l(kr) - \frac{1}{k} \partial_r h_l(kr), \quad (19)$$

and the defining equation for the spherical hankel functions, to find

$$F_l(r) = \frac{r^2}{2\tilde{k}_\mu^2} \left( h_l(n_B \tilde{k}_\mu r) \partial_r (r \partial_r h_l(n_B \tilde{k}_\mu r)) - r (\partial_r h_l(n_B \tilde{k}_\mu r))^2 \right). \quad (20)$$

Inserting in Eq. (7) and rearranging the terms by multiplying onto the spherical harmonics, we can write the angular integration as a surface integral in terms of the QNMs in the exact form of Eq. (17).

## III. EXAMPLE CALCULATIONS

In this section we present a number of example calculations to illustrate that the three formulations give the same value for the norm in practical calculations. First, we consider the case of a homogeneous sphere, for which the functional form of the QNMs are known analytically and we can carry out the regularization of Eq. (5) explicitly. This example was also considered by Muljarov *et al.* in Ref. 12. Next, we revisit the photonic crystal cavity of Ref. 5 and the plasmonic nanorod dimer of Ref. 22 to elaborate on the practical evaluation of Eq. (5).

### A. Homogeneous sphere

As a first set of example applications of the three formulations, we consider QNMs of homogeneous spheres with radius  $a$  in air. Following Muljarov *et al.*, we consider electric field QNMs of the transverse kind which may be written, for positions outside the sphere, in terms

of the vector spherical harmonics  $\Phi_{lm}(\theta, \varphi)$  as

$$\tilde{\mathbf{f}}_{lm}(\mathbf{r}) = h_l(\tilde{k}_\mu r) \Phi_{lm}(\theta, \varphi), \quad (21)$$

where  $\Phi_{lm}(\theta, \varphi) = \mathbf{r} \times \nabla Y_{lm}$ , and  $Y_{lm}$  denotes the (scalar) spherical harmonic. For simplicity, we limit the discussion to the case of  $l = 1$  for which the spherical Hankel function may be written explicitly as

$$h_1(z) = -(z + i) \frac{e^{iz}}{z^2}. \quad (22)$$

Inserting in Eq. (5) it follows that

$$\begin{aligned} \langle \langle \tilde{\mathbf{f}}_{1m} | \tilde{\mathbf{f}}_{1m} \rangle \rangle_{\text{Lai}} &= I_{1m}^{r < a} + 2 \left( \frac{i}{2\tilde{k}_\mu^3} - \frac{1}{\tilde{k}_\mu^4 a} \right) e^{2i\tilde{k}_\mu a} \\ &+ \lim_{R \rightarrow \infty} \{f_{\text{Lai}}^{\text{res}}(R)\}, \end{aligned} \quad (23)$$

where

$$I_{1m}^{r < a} = \int_0^a \int_\Omega \epsilon_r(\mathbf{r}) \tilde{\mathbf{f}}_{1m}(\mathbf{r}) \cdot \tilde{\mathbf{f}}_{1m}(\mathbf{r}) dV \quad (24)$$

denotes the integral over the finite sphere, and the residual  $R$  dependent factor is

$$f_{\text{Lai}}^{\text{res}}(R) = -\frac{i}{\tilde{k}_\mu^5 R^2} e^{2i\tilde{k}_\mu R}. \quad (25)$$

By rewriting the norm as in Eq. (12) we can regularize the integral and conclude that the norm is

$$\langle \langle \tilde{\mathbf{f}}_{1m} | \tilde{\mathbf{f}}_{1m} \rangle \rangle_{\text{Lai}} = I_{1m}^{r < a} + 2 \left( \frac{i}{2\tilde{k}_\mu^3} - \frac{1}{\tilde{k}_\mu^4 a} \right) e^{2i\tilde{k}_\mu a}. \quad (26)$$

In a similar way, we can evaluate Eq. (16) to find that

$$\begin{aligned} \langle \langle \tilde{\mathbf{f}}_{1m} | \tilde{\mathbf{f}}_{1m} \rangle \rangle_{\text{Sauvan}} &= I_{1m}^{r < a} + 2 \left( \frac{i}{2\tilde{k}_\mu^3} - \frac{1}{\tilde{k}_\mu^4 a} \right) e^{2i\tilde{k}_\mu a} \\ &+ \lim_{R \rightarrow \infty} \{f_{\text{Sauvan}}^{\text{res}}(R)\}, \end{aligned} \quad (27)$$

where

$$f_{\text{Sauvan}}^{\text{res}}(R) = \left( \frac{1}{\tilde{k}_\mu^6 R^3} - \frac{2i}{\tilde{k}_\mu^5 R^2} \right) e^{2i\tilde{k}_\mu R}. \quad (28)$$

Clearly, Eq. (27) can be regularized in way completely analogous to Eq. (23), which is nothing but a different way of introducing the coordinate transform that was performed by use of PMLs in Ref. 11. With this approach, one finds immediately that the two norms are identical.

Finally, using Eq. (17) one can directly verify that

$$\langle \langle \tilde{\mathbf{f}}_{1m} | \tilde{\mathbf{f}}_{1m} \rangle \rangle_{\text{Muljarov}} = I_{1m}^{r < a} + 2 \left( \frac{i}{2\tilde{k}_\mu^3} - \frac{1}{\tilde{k}_\mu^4 a} \right) e^{2i\tilde{k}_\mu a}, \quad (29)$$

so that it equals the result of the other two formulations of the norm — without an explicit need for regularization.

## B. Photonic crystal cavity

As a second example, we consider the simple two dimensional photonic crystal cavity of Ref. 5, which is formed by six cylinders of relative permittivity  $\epsilon_{\text{rods}} = 11.4$  in air. The cylinders are arranged in a hexagon with side length  $a$  and have radii  $r = 0.15a$ . We consider the out-of-plane polarization, for which the cavity supports a QNM  $\tilde{\mathbf{f}}_c(\mathbf{r})$  with complex resonance frequency  $\tilde{\omega}_c a / 2\pi c = 0.425862 - 0.013539i$ , corresponding to  $Q \approx 16$ . Figure 2 shows the real part of  $\tilde{\mathbf{f}}_c(\mathbf{r})$  which is scaled to unity in the cavity center  $\mathbf{r}_c = (0, 0)$ .

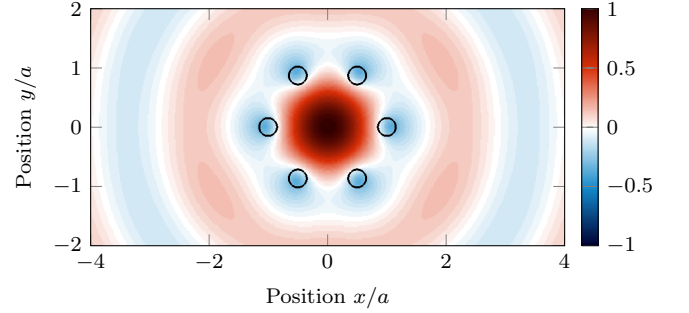


FIG. 2: Real part of the fundamental QNM  $\tilde{\mathbf{f}}_c(\mathbf{r})$  in a small cavity made from high-index rods arranged in a hexagon with side length  $a$ , as indicated by black circles. The QNM is scaled to unity in the cavity center  $\mathbf{r}_c = (0, 0)$ .

For these QNM calculations, we used a Fredholm type integral equation in which the QNMs appear as the self-consistent solutions to a scattering problem with no incident field<sup>5</sup>. The equation was solved by an iterative procedure in which, for each guess of a resonance frequency  $\tilde{\omega}_{\text{guess}}$ , we set up the integral equation and solved it to find the eigenvalue closest to  $\tilde{\omega}_{\text{guess}}$ ; the iterations then continued until the difference was smaller than some prescribed tolerance. Specifically, for each  $\tilde{\omega}_{\text{guess}}$ , we discretized the integral eigenvalue equation by expanding the background Green tensor and the unknown field within each rod in a basis of cylindrical wave functions<sup>23</sup>. Owing to the inherent wave nature of the basis functions, each with the frequency  $\tilde{\omega}_{\text{guess}}$ , this basis is particularly well suited for the expansion, and the integral formulation in terms of the Green tensor means that the radiation condition is inherently satisfied. In total, this enables very high accuracy calculations of QNMs, although the method is best suited to collections of cylindrical<sup>23</sup> or spherical<sup>24</sup> scatterers for which the projections onto the basis functions simplify significantly.

To help in the following discussion, it is worth distinguishing between the generalized effective mode volume, defined formally in Eq. (3) as a single complex number, and the numerically calculated number  $v_i^{\text{num}}(R)$ , with  $i \in \{\text{Lai}, \text{Muljarov}\}$ , that is obtained from Eq. (3) by substituting the corresponding normalization formulas calculated in a circular domain of radius  $R$ . The upper panel of Fig. 3 shows a zoom in at the real part

of  $v_{\text{Lai}}^{\text{num}}(R)$  in which an oscillatory behavior is clearly visible; from the discussion in Section II A, we can associate these oscillations with the residual  $R$ -dependent term  $f_{\text{Lai}}^{\text{res}}(R)$ . A minimum in the oscillation amplitudes occurs at  $R \approx 15a$ , after which the amplitudes increase without bounds as  $R \rightarrow \infty$ .

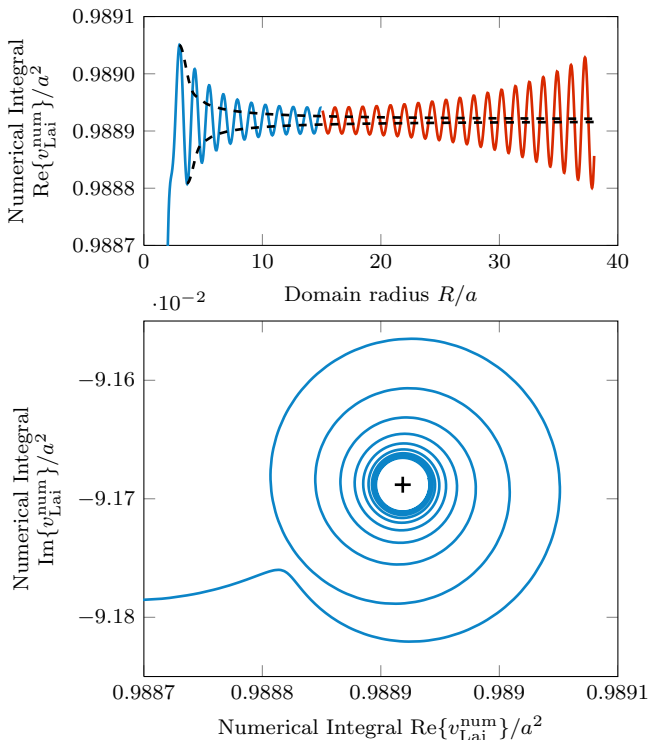


FIG. 3: Top: Real part of the calculated generalized effective mode volume as function of calculation domain radius  $R$ . Blue and red parts of the curve indicate the regions in which the oscillations decrease and increase in magnitude, respectively. Black dashed curves show the second order running averages starting from the first local maximum and minimum. Bottom: Values of the calculated generalized effective mode volume as a parameterized function of calculation domain radius  $R$  for the part of the curve with decreasing oscillation amplitudes,  $2a < R < 15a$ . The center of the innermost circle corresponds to the generalized effective mode volume and is indicated with a cross.

An illustrative alternative display of the oscillatory behavior of  $v_{\text{Lai}}^{\text{num}}(R)$  is found by plotting the values in the complex frequency plane as shown in the lower panel of Fig. 3. In this way one can quite easily appreciate how the values of  $v_{\text{Lai}}^{\text{num}}(R)$  spirals initially towards a fixed value until the complex exponential factor in  $f_{\text{Lai}}^{\text{res}}(R)$  takes over and causes the values to spiral outwards. We find that the qualitative behavior of  $v_{\text{Lai}}^{\text{num}}(R)$  in the form of a spiral is not affected by the accuracy of the calculations, but the center of the spiral is. The oscillating behavior provides a convenient and very graphical means of regularizing the integral by simply determining the center of the spiral. Clearly, this can be done with an accuracy which is much better than the smallest oscillation magni-

tude (better than the radius of the innermost circle in the spiral). Therefore, for all practical purposes, the error in the calculated value of  $v_Q$ , in this case, is dominated by the numerical integration and not the regularization of the integral.

In practical calculations we find that one can get a convenient high-accuracy estimate of the center of the spiral by calculating the moving average

$$v_Q^{(n)}(R_N) = \frac{1}{N} \sum_{n=n_0}^N v_Q^{(n-1)}(R_n), \quad (30)$$

where  $v_Q^{(0)}(R_n)$  denotes the  $n$ 'th calculated value of  $v_{\text{Lai}}^{\text{num}}(R)$ . In the present case of the photonic crystal cavity, the second order moving average  $v_Q^{(2)}$  shows a smooth behavior for  $0 < R/a < 40$ , and by choosing two different starting points  $n_0$ , corresponding to consecutive local maxima and minima of the curve of  $v_{\text{Lai}}^{\text{num}}(R)$ , we get corresponding upper and lower bounds for  $v_Q$ , as illustrated in Fig. 3. Because of the exponentially increasing factor in  $f_{\text{Lai}}^{\text{res}}(R)$ , the running averages will in general not tend to zero at large distances, but may eventually start increasing (exponentially). Therefore, we do not consider their use to be a formal regularization procedure in itself, but rather a simple computational method for estimating the center of the spiral. With this procedure we find the value

$$v_Q/a^2 = 0.988918 - 0.091688i, \quad (31)$$

with an estimated error of  $|\delta v_Q|/a^2 < 2 \times 10^{-6}$ . The oscillating behavior in Fig. 3 is exactly what was noted in Ref. 5 which stated that “For very low- $Q$  cavities, however, the convergence is nontrivial due to the exponential divergence of the modes that may cause the inner product to oscillate around the proper value as a function of calculation domain size”. In practice, the magnitude of the oscillations are often much smaller than the desired accuracy for positions within typical calculation domains, and may also be much smaller than the overall numerical accuracy.

Next, we compare to results of calculations based on the formulation by Muljarov *et al.*. Notably, in Eq. (17) there is no requirement of an infinite calculation domain, which is very convenient from a numerical point of view. For the practical implementation, however, one must evaluate (numerically) both the first and the second derivative; together with the general accuracy of the integral, the accuracy of the derivatives then governs the overall precision. Because of the finite accuracy in the calculations there is a numerically induced phase difference between the two terms in Eq. (17), wherefore the changes in the volume integral is not fully compensated by the surface term. This difference becomes more pronounced at larger values of  $R$ , because the derivatives become larger. Instead of investigating the behavior of Eq. (17) as a function of calculation domain size as in Fig. 3, we take a fixed calculation domain size of  $R = 2a$

and evaluate the integrals with a fixed relative accuracy of  $|\delta v_{\text{Muljarov}}^{\text{num}}|/a^2 = 10^{-7}$  and first order finite difference approximations to the derivatives calculated using successively smaller differences  $\Delta r$ . The results are shown in Table I and display a convergent behavior towards a value consistent with the calculation using the formulation of Lai *et al.*, cf. Eq. (31).

$\Delta r/a$	$v_{\text{Muljarov}}^{\text{num}}(2a)/a^2$
0.01	0.988894 - 0.091660i
0.001	0.988918 - 0.091688i
0.0001	0.988918 - 0.091688i

TABLE I: Values of the calculated generalized effective mode volume  $v_{\text{Muljarov}}^{\text{num}}(2a)$  for a fixed calculation domain size  $R = 2a$  and relative integration tolerance  $\delta v_{\text{Muljarov}}^{\text{num}}/a^2 = 10^{-7}$  but varying accuracy of the numerical derivatives.

### C. Plasmonic nanorod dimer

As a final example, we consider the three dimensional metallic nanorod dimer in Fig. 1, which was recently studied in Ref. 22. It consists of two gold nanorods of length 100 nm and radius  $r_{\text{rod}} = 15$  nm in a homogeneous background with refractive index  $n_B = 1.5$ . The gold nanorods are aligned along the same axis and spaced by a gap of 20 nm. The relative permittivity of the gold nanorods is modeled as

$$\epsilon_{\text{rod}}(\omega) = 1 - \frac{\omega_p^2}{\omega^2 + i\omega\gamma}, \quad (32)$$

with  $\omega_p = 1.26 \times 10^{16}$  rad/s, and  $\gamma = 1.41 \times 10^{14}$  rad/s. The resonance frequency of the dipolar like QNM of interest is  $\tilde{\omega}/2\pi = (291 - i20.3)$  THz, corresponding to the wavelength  $\tilde{\lambda} = 2\pi c/\tilde{\omega} = (1025 + 72i)$  nm and a quality factor of  $Q \approx 7.2$ .

These QNM calculations were performed using the finite-difference time-domain (FDTD) method (Lumerical FDTD solutions<sup>25</sup>). We used a spatial plane wave excitation near 291 THz with polarization along the dimer axis and a 6 fs Gaussian temporal profile as well as a run-time Fourier transform to obtain the spatial distribution of the QNM. As is common practise in FDTD when analyzing metals and other high index materials, we used a non-uniform mesh consisting of relatively small cubic Yee cells of side length 1 nm for the inner region and larger cells of side length 50 nm for the outer region. See Ref. 22 for further calculation details. Despite the fine discretization, we expect the overall accuracy of these calculations to be limited to approximately 1% due to meshing, sub-meshing and numerical dispersion in FDTD, which is known to be particularly demanding for metallic structures<sup>26</sup>. We consider these to be state-of-the-art gridding parameters for metal resonators using

FDTD, with simulation times on the order of days on a small computer cluster.

As in the case of the two-dimensional cavity, we can investigate the variation in the calculated generalized effective mode volume with calculation domain size. To this end, we define the center position  $\mathbf{r}_c$  as the point directly between the two nanorods and evaluate Eq. (5), with the substitution  $\epsilon_r(\mathbf{r}) \rightarrow \sigma(\mathbf{r}, \tilde{\omega}_\mu)$ , in a rectangular cuboid of side lengths  $L_x = L_z$  and  $L_y = 3.5 \mu\text{m}$  completely enclosing the dimer. Figure 4 shows the variation in  $v_{\text{Lai}}^{\text{num}}$  as a function of domain width  $L_x$ . The variation in the numerical integral shows a clear oscillation as in Fig. 2, although the spiraling behavior is less symmetric. Despite the lower symmetry of the spiral, which we attribute to the lower degree of symmetry of the cuboidal integration domain, we can use the second order running averages to determine the center of the oscillation with relatively high precision. With this approach, we find

$$v_Q/r^3 = 35.19 - 0.96i, \quad (33)$$

with an estimated error of  $|\delta v_Q| < 0.1r^3$ . This estimate, which is indicated by the gray shaded areas in Fig. 4, is more conservative than what would follow directly from the curves of the second order running averages because of the numerical quadrature and the lesser degree of symmetry. Nevertheless, the error is still much smaller than the expected overall numerical accuracy in the FDTD calculations, wherefore the error of the calculated  $v_Q$  also in this case is expected to be dominated by the error in the numerical calculations and not the regularization. The generalized effective mode volume in Eq. (33) leads to an enhanced spontaneous emission rate  $\Gamma$ , relative to the rate in the homogeneous background,  $\Gamma_B$ , of  $\Gamma/\Gamma_B = 1475 \pm 8$ , as calculated using a single QNM approximation to the Green tensor<sup>4</sup>. The stated uncertainty is on the order of 0.5% and is a simple estimate calculated as the difference in the extremal Purcell factors resulting from the finite accuracy of  $v_Q$ . Assuming negligible quasi-static coupling, we can assess this value by comparing to independent reference calculations of the spontaneous emission rate using FDTD to determine the electric field Green tensor. With this approach we find  $\Gamma^{\text{ref}}/\Gamma_B = 1484 \pm 2$ . These reference calculations were performed with the same mesh as the QNM calculation, wherefore we expect the overall intrinsic numerical error due to discretization to be less important for the comparison. The two independent calculations agree to within the estimated errors; notably, the QNM approach predicts a value that is lower than the reference calculation, which is consistent with the possibility of non-vanishing quasi-static coupling due to the proximity of  $\mathbf{r}_c$  to the metal surfaces.

In closing, we would like to remark that we have found Eq. (17) difficult to evaluate with FDTD data to a precision in which it provides better accuracy than Eq. (5). We believe that these problems are likely caused by the finite accuracy of the QNM calculation, which in practice is an unfortunate but rather general characteristic of



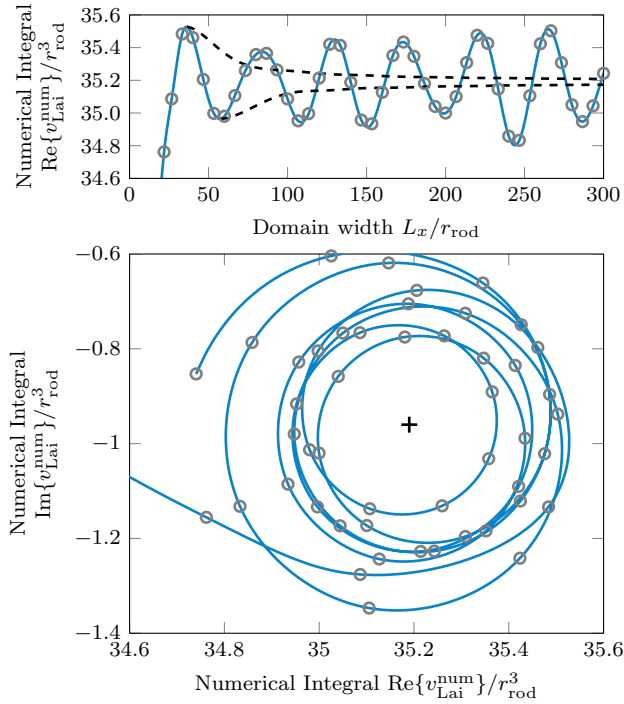


FIG. 4: Top: Real part of the calculated generalized effective mode volume as function of calculation domain width  $L_x$ . Gray shaded area shows the estimated uncertainty in the determination of  $v_Q$ . Bottom: Values of the calculated generalized effective mode volume as a parameterized function of calculation domain radius. The full curve is a spline-interpolation of the calculated data points shown by gray circles. The generalized effective mode volume  $v_Q$  is indicated with a cross, and the estimated uncertainty is indicated with the gray shading.

many numerical Maxwell solvers in three dimensions. For FDTD, the inherent formulation in terms of Cartesian coordinates may also lead to additional interpolation errors when performing the radial differentiation as dictated by Eq. (17). In the present case of the plasmonic dimer, in particular, we found that the large field gradients lead to relatively large numerical errors in the surface integral which in practice dominates the achievable accuracy.

### Discussion

Comparing Eqs. (5), (14) and (17), we can understand the three formulations of the norm as arising from three different approaches to the regularization of the integral

$$\int \epsilon_r(\mathbf{r}) \tilde{\mathbf{f}}_\mu(\mathbf{r}) \cdot \tilde{\mathbf{f}}_\mu(\mathbf{r}) dV. \quad (34)$$

This integral can be regularized immediately by a complex coordinate transform, as discussed in section II A. Therefore, in view of Eqs. (17) one may view the surface term in Eq. (5) as a simple choice of regularization for use with data at positions along the real axis. It is worth

noting, however, that the surface term appears directly in perturbation theory calculations<sup>6</sup>, or from Eq. (16), under the assumption of the Silver-Müller radiation condition, and it is in principle important for the argument based on Eqs. (10) or (16) that one can assign a well-defined value to the norm as  $R \rightarrow \infty$ . In many practical calculations we find that the relatively simple formula of Lai *et al.* is very often sufficient, and that the uncertainty in the norm (or the associated effective mode volume) is dominated by the uncertainty in the numerical data. When one has access to complex position data, the normalization of Sauvan *et al.* represents an obvious alternative, and for high-accuracy numerical data, or when the QNMs are known analytically, one can benefit the most from the formula of Muljarov *et al.*

In this Article, we have focused on normalization of resonators embedded in a homogeneous background material, for which we have argued that Eq. (2) represents the proper choice of radiation condition. For resonators coupled to waveguides the radiation condition is different, but also in this case there appears to be an inherent need for regularization of the normalization integral<sup>27</sup>. Also, it is worth noting that Bai *et al.* recently introduced an alternative calculation method for QNMs, based on a scattering formulation at complex frequencies, in which the resulting QNMs are inherently normalized without an explicit need for an integration step<sup>28</sup>.

## IV. CONCLUSIONS

In conclusion, we have discussed the relation between three different formulations for the normalization of QNMs in leaky optical cavities and plasmonic resonators. The three formulations arise from independent derivations of an expansion for the electromagnetic field in terms of QNMs, and for spherical calculation volumes, we have shown the equivalence between the different formulas explicitly. We have argued, that the apparent differences in the normalization formulas can be understood as arising from alternative ways of regularizing the normalization integral to handle the inherently divergent QNMs. In this view, the surface term in the normalization by Lai *et al.* represents a simple choice of regularization which in principle is insufficient to properly regularize the integral when the size of the calculation domain is varied along the real axis. We have discussed this issue in detail, and we have shown how one can, in principle, always regularize the integral by a complex coordinate transform. In practice, we find that there is rarely any need for additional regularization beyond the relatively simple formula of Lai *et al.* Nevertheless, depending on the calculation method used to obtain the QNMs, the normalizations of Sauvan *et al.* or Muljarov *et al.* may be more convenient. Regardless of the choice of normalization integral, we have discussed how one can use the norm to define an effective mode volume for use in the Purcell



formula. Because of the complementarity of the three norms, this naturally leads to the same estimates of the enhanced spontaneous emission factor.

This work was supported by the Carlsberg foundation, Queen's University and the Natural Sciences and Engineering Research Council of Canada.

- 
- <sup>1</sup> Purcell, E. M. *Spontaneous Emission Probabilities at Radio Frequencies*. Physical Review **69**, 681 (1946).
  - <sup>2</sup> Ching, E. S. C., Leung, P. T. & Young, K. *Optical processes in microcavities—the role of quasi-normal modes*, R. K. Chang and A. J. Campillo Eds. (World Scientific, 1996).
  - <sup>3</sup> Ching, E. S. C., Leung, P. T., Maassen van den Brink, A., Suen, W. M., Tong, S. S. & Young, K. *Quasinormal-mode expansion for waves in open systems*. Review of Modern Physics **70**, 1545–1554 (1998).
  - <sup>4</sup> Kristensen, P. T. & Hughes, S. *Modes and Mode Volumes of Leaky Optical Cavities and Plasmonic Nanoresonators*. ACS Photonics **1**, 2–10 (2014).
  - <sup>5</sup> Kristensen, P. T., Vlack, C. V. & Hughes, S. *Generalized effective mode volume for leaky optical cavities*. Optics Letters **37**, 1649–1651 (2012).
  - <sup>6</sup> Lai, H. M., Leung, P. T., Young, K., Barber, P. W. & Hill, S. C. *Time-independent perturbation for leaking electromagnetic modes in open systems with application to resonances in microdroplets*. Physical Review A **41**, 5187–5198 (1990).
  - <sup>7</sup> Leung, P. T., Liu, S. Y. & Young, K. *Completeness and orthogonality of quasinormal modes in leaky optical cavities*. Physical Review A **49**, 3057–3067 (1994).
  - <sup>8</sup> Leung, P. T. & Pang, K. M. *Completeness and time-independent perturbation of morphology-dependent resonances in dielectric spheres*. Journal of the Optical Society of America B **13**, 805 (1996).
  - <sup>9</sup> Lee, K. M., Leung, P. T. & Pang, K. M. *Dyadic formulation of morphology-dependent resonances. I. Completeness relation*. Journal of the Optical Society of America B **16**, 1409–1417 (1999).
  - <sup>10</sup> Lee, K. M., Leung, P. T. & Pang, K. M. *Dyadic formulation of morphology-dependent resonances. II. Perturbation theory*. Journal of the Optical Society of America B **16**, 1418–1430 (1999).
  - <sup>11</sup> Sauvan, C., Hugonin, J. P., Maksymov, I. S. & Lalanne, P. *Theory of the Spontaneous Optical Emission of Nano-size Photonic and Plasmon Resonators*. Physical Review Letters **110**, 237401 (2013).
  - <sup>12</sup> Muljarov, E. A., Doost, M. B. & Langbein, W. *Exact mode volume and Purcell factor of open optical systems*. arXiv:1409.6877 [cond-mat.mes.hall] (2014).
  - <sup>13</sup> Muljarov, E. A., Langbein, W. & Zimmermann, R. *Brillouin-Wigner perturbation theory in open electromagnetic systems*. European Physics Letters **92**, 50010 (2010).
  - <sup>14</sup> Martin, P. *Multiple Scattering. Interaction of time-harmonic waves with N obstacles* (Cambridge University Press, 2006).
  - <sup>15</sup> Koenderink, A. F. *On the use of Purcell factors for plasmon antennas*. Optics Letters **35**, 4208–4210 (2010).
  - <sup>16</sup> Ge, R.-C., Kristensen, P. T., Young, J. F. & Hughes, S. *Quasinormal mode approach to modelling light-emission and propagation in nanoplasmonics*. New Journal of Physics **16**, 113048 (2014).
  - <sup>17</sup> Zel'dovich, Y. B. *On the theory of unstable states*. Soviet Physics JETP **12**, 542 (1961).
  - <sup>18</sup> Barrera, R. G., Estévez, G. A. & Giraldo, J. *Vector spherical harmonics and their application to magnetostatics*. European Journal of Physics **6**, 287 (1985).
  - <sup>19</sup> Snyder, A. W. & Love, J. *Optical Waveguide Theory* (1983).
  - <sup>20</sup> Lecamp, G., Hugonin, J. P. & Lalanne, P. *Theoretical and computational concepts for periodic optical waveguides*. Optics Express **15**, 11042–11060 (2007).
  - <sup>21</sup> Tai, C.-T. *Dyadic Green Functions in Electromagnetic Theory*, 2nd ed. (IEEE Press, 1994).
  - <sup>22</sup> Ge, R.-C. & Hughes, S. *Design of an efficient single photon source from a metallic nanorod dimer: a quasi-normal mode finite-difference time-domain approach*. Optics Letters **39**, 4235 (2014).
  - <sup>23</sup> Kristensen, P. T., Lodahl, P. & Mørk, J. *Light propagation in finite-sized photonic crystals: Multiple scattering using an electric field integral equation*. Journal of the Physical Society of America B **27**, 228–237 (2010).
  - <sup>24</sup> de Lasson, J. R., Mørk, J. & Kristensen, P. T. *Three-dimensional integral equation approach to light scattering, extinction cross sections, local density of states, and quasinormal modes*. Journal of the Optical Society of America B **30**, 1996–2007 (2013).
  - <sup>25</sup> We used FDTD solutions V. 8.6.3, www.lumerical.com.
  - <sup>26</sup> Vlack, C. V. *Dyadic Green Functions and their applications in Classical and Quantum Nanophotonics*. Ph.D. thesis, Queen's University (2012).
  - <sup>27</sup> Kristensen, P. T., de Lasson, J. R. & Gregersen, N. *Calculation, normalization, and perturbation of quasinormal modes in coupled cavity-waveguide systems*. Optics Letters **39**, 6359 (2014).
  - <sup>28</sup> Bai, Q., Perrin, M., Sauvan, C., Hugonin, J.-P. & Lalanne, P. *Efficient and intuitive method for the analysis of light scattering by a resonant nanostructure*. Optics Express **21**, 27371–27382 (2013).